Dark matter flow dataset Part II: Correlation-based statistics from cosmological N-body simulation

Zhijie (Jay) Xu,[1]★

[1]*Physical and Computational Sciences Directorate, Pacific Northwest National Laboratory; Richland, WA 99352, USA*

ABSTRACT

Dark matter (DM), if exists, is believed to be cold, collisionless, dissipationless, non-baryonic, barely interacting with baryonic matter except through gravity, and sufficiently smooth on large scales with a fluid-like behavior. The flow of dark matter can be best described by a self-gravitating collisionless fluid dynamics (SG-CFD). The statistics of dark matter density, velocity, acceleration, energy, momentum, and their redshift evolution play essential roles for structure formation and evolution. These information can be systematically extracted from cosmological N-body simulations by either i) a structural (halo-based) or ii) a statistical (correlation-based) approach. In this correlation-based statistical dataset, i) all particle pairs with any given separation r in N-body system are identified; ii) statistical measures are calculated over all particle pairs with the same separation r (pairwise average); iii) the redshift (z) and scale (r) dependence of all statistical measures (correlation/moment/structure/dispersion/spectrum functions for density, velocity and potential etc.) are presented.

Key words: Cosmology; Dark matter; N-body simulations; Correlation-based statistics;

1 INTRODUCTION

The cosmic peculiar velocity, acceleration, density, and potential fields contain rich information for the dynamics of self-gravitating collisionless dark matter flow (SG-CFD) from large scale to the highly non-linear small scales. Statistics of velocity, acceleration, density, and potential fields are crucial for understanding structure formation and dynamics. While direct measuring from real samples is still challenging in practice, tremendous information can be obtained from N-body simulations.

However, it is not trivial to extract statistics from N-body simulations. Particle velocity and density are only sampled at discrete locations. That sampling has a poor quality at locations with low particle density. The standard approach computes the power spectrum in Fourier space, where cloud-in-cell (CIC) or triangular-shaped-cloud (TSC) schemes are used to project fields onto regular grids. This will introduce sampling errors.

Since both real-space and Fourier-space data contain the same information, directly working in real-space avoids the information distortion due to field projection and the conversion between Fourier- and real-space. This dataset presents the real-space correlation-based statistics for dark matter flow that was obtained directly from simulation without field projection. It was later used to develop the statistical theory including

(i) Kinematic relations, flow characterization, and correlation /structure /dispersion /spectrum functions on different scales (Xu 2022e)
(ii) General kinematic relations and dynamic relations on large and small scales for correlations of same or different order (Xu 2022f)

(iii) Scale and redshift dependence of velocity and density distributions on small, intermediate, and large scales (Xu 2022h)
(iv) Generalized Stable clustering hypothesis for pairwise velocity on small scale (Xu 2021d)

along with three applications of dark matter flow

(i) Predicting Dark matter particle mass and properties from energy cascade in dark matter flow (Xu 2022i)
(ii) Origin of MOND acceleration and deep-MOND from acceleration fluctuation and energy cascade in dark matter flow (Xu 2022j)
(iii) Baryonic-to-halo mass relation from mass and energy cascade in dark matter flow (Xu 2022k)

Presentation slides accompanying this dataset, "A comparative study of dark matter flow & hydrodynamic turbulence and its applications", can be found at (Xu 2022a). A relevant dataset for halo-based statistics of dark matter flow can be found at (Xu 2022b), which is used for developing the theory of mass and energy cascade (Xu 2021a,b,f, 2022d, 2021c,e, 2022g). All data files are also available on GitHub (Xu 2022c).

2 N-BODY SIMULATIONS AND NUMERICAL DATA

The simulation data used to generate this dataset is public available from large-scale *N*-body simulations carried out by the Virgo consortium. A comprehensive description of the data can be found in (Frenk et al. 2000). Current study is carried out using simulations with $\Omega_0 = 1$ and the standard CDM power spectrum (SCDM) to focus on the matter-dominant (Einstein–de Sitter) gravitational collapse. The same set of data has been widely used in a number of studies from clustering statistics to the formation of cluster halos in

---

★ E-mail: zhijie.xu@pnnl.gov; zhijiexu@hotmail.com

Table 1. Numerical parameters of N-body simulation

Run	Ω_0	Λ	h	Γ	σ_8	L (Mpc/h)	N	m_p $M_\odot/h$	l_{soft} (Kpc/h)
SCDM1	1.0	0.0	0.5	0.5	0.51	239.5	256^3	2.27×10^{11}	36
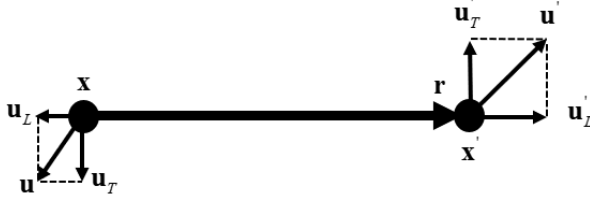
Figure 1. Sketch of longitudinal and transverse velocities, where $\mathbf{u}_T$ and $\mathbf{u}'_T$ are transverse velocities at two locations $\mathbf{x}$ and $\mathbf{x}'$. u_L and u'_L are two longitudinal velocities. Correlation-based statistics in this dataset is presented as the average of a given variable for all particle pairs with the same separation r. Therefore, various statistical measures are presented as functions of scale r and redshift z.

large scale environments, and halo abundances and mass functions. Key simulation parameters are provided in Table 1.

In this correlation-based statistical dataset, a non-projection approach is used for statistical analysis instead of projecting particle fields onto structured grid: i) all particle pairs with any given separation r in N-body system are identified; This will maximally preserve and utilize the information from N-body simulation; ii) statistical measures are calculated over all particle pairs with the same separation r (pairwise average); iii) the redshift (z) and scale (r) dependence of all statistical measures (correlation/moment/structure/dispersion/spectrum functions for density, velocity and potential etc.) are presented.

Figure 1 is a schematic plot of pair of particles on scale r. Statistical analysis is performed over transverse velocities (u_T and u'_T), longitudinal velocities (u_L and u'_L), velocity difference or pairwise velocity ($\Delta u_L = u_{L'} - u_L$) and velocity sum ($\Sigma u_L = u_{L'} + u_L$). Figure 2 lists the two-point velocity correlation functions of different order (p,q) that can be computed from the velocities in Fig. 1.

3 OVERVIEW

Correlation-based statistical data in this package was generated from large scale N-body simulations and saved in a format of CSV file.

3.1 Data Availability

The data underlying this article are available in Zenodo at Dark matter flow dataset Part II: Correlation-based statistics from cosmological N-body simulation, along with the accompanying presentation slides "A comparative study of dark matter flow & hydrodynamic turbulence and its applications" (Xu 2022a). All data files are also available on GitHub (Xu 2022c).

- ☒ All data **are** publicly available.
- ☐ Some data **cannot be made** publicly available.
- ☐ **No data can be made** publicly available.

3.2 Dataset list

Table 2 lists all data files included in this dataset. Every data file presents the scale (r) and redshift (z) dependence of one statistical measures with symbols also listed in the same table. The physical meaning of that variable can be found from the name of file. More details (definition, units, relevant publications, equations, and figures) can be found in the header of each data file.

REFERENCES

Frenk C. S., et al., 2000, arXiv:astro-ph/0007362v1
Xu Z., 2021a, arXiv e-prints, p. arXiv:2109.09985
Xu Z., 2021b, arXiv e-prints, p. arXiv:2109.12244
Xu Z., 2021c, arXiv e-prints, p. arXiv:2110.03126
Xu Z., 2021d, arXiv e-prints, p. arXiv:2110.05784
Xu Z., 2021e, arXiv e-prints, p. arXiv:2110.09676
Xu Z., 2021f, arXiv e-prints, p. arXiv:2110.13885
Xu Z., 2022a, A comparative study of dark matter flow & hydrodynamic turbulence and its applications, doi:10.5281/zenodo.6569901, http://dx.doi.org/10.5281/zenodo.6569901
Xu Z., 2022c, Dark matter flow dataset, doi:10.5281/zenodo.6586212, https://github.com/ZhijieXu2022/dark_matter_flow_dataset
Xu Z., 2022b, Dark matter flow dataset Part I: Halo-based statistics from cosmological N-body simulation, doi:10.5281/zenodo.6541230, http://dx.doi.org/10.5281/zenodo.6541230
Xu Z., 2022d, arXiv e-prints, p. arXiv:2201.12665
Xu Z., 2022e, arXiv e-prints, p. arXiv:2202.00910
Xu Z., 2022f, arXiv e-prints, p. arXiv:2202.02991
Xu Z., 2022g, arXiv e-prints, p. arXiv:2202.04054
Xu Z., 2022h, arXiv e-prints, p. arXiv:2202.06515
Xu Z., 2022i, arXiv e-prints, p. arXiv:2202.07240
Xu Z., 2022j, arXiv e-prints, p. arXiv:2203.05606
Xu Z., 2022k, arXiv e-prints, p. arXiv:2203.06899

Table 2. List of data files in correlation-based dataset for dark matter flow

Data file (*.csv)	Symbol	Reference	Eq.	Fig.
1_Cos_longitudinal_angle_ang_uL_uLs	$\cos\theta_L$	(Xu 2022e)	(21)	17
2_Cos_transverse_angle_ang_uT_uTs	$\cos\theta_T$	(Xu 2022e)	(21)	17
3_Cos_vel_r_angle ang_u_r	$\cos\theta_{ur}$	(Xu 2022e)	(22)	17
4_Density_correlation_function_kesi	$\xi(r,z)$	(Xu 2022h)	(9)	6,8
5_Density_dispersion_function_Sigma2_d	$\sigma_\delta^2(r,z)$	(Xu 2022h)	(24)(35)	11
6_Density_fluctuation_distribution_E_dr	$E_{\delta r}(r,z)$	(Xu 2022h)	(30)	12
7_Enstrophy_distribution_function_E_nr	$E_{nr}(r,z)$	(Xu 2022e)	(78)	13
8_Kinetic_energy_distribution_E_ur	$E_{ur}(r,z)$	(Xu 2022e)	(32)	11
9_Longitudinal_velocity_correlation_rho_L	$\rho_L(r,z)$	(Xu 2022e)	(20)	16
10_Longitudinal_velocity_generalized_kurtosis_K3	$K_3(\Delta u_L, r)$	(Xu 2022h)	(37)	
11_Longitudinal_velocity_generalized_kurtosis_K4	$K_4(\Delta u_L, r)$	(Xu 2022h)	(37)	15
12_Longitudinal_velocity_generalized_kurtosis_K5	$K_5(\Delta u_L, r)$	(Xu 2022h)	(37)	
13_Longitudinal_velocity_generalized_kurtosis_K6	$K_6(\Delta u_L, r)$	(Xu 2022h)	(37)	15
14_Longitudinal_velocity_generalized_kurtosis_K7	$K_7(\Delta u_L, r)$	(Xu 2022h)	(37)	
15_Longitudinal_velocity_generalized_kurtosis_K8	$K_8(\Delta u_L, r)$	(Xu 2022h)	(37)	15
16_Longitudinal_velocity_sum_generalized_kurtosis_K4	$K_4(\Sigma u_L, r)$	(Xu 2022h)	(37)	15
17_Longitudinal_velocity_sum_generalized_kurtosis_K6	$K_6(\Sigma u_L, r)$	(Xu 2022h)	(37)	15
18_Longitudinal_velocity_sum_generalized_kurtosis_K8	$K_8(\Sigma u_L, r)$	(Xu 2022h)	(37)	15
19_Pairwise_velocity_generalized_kurtosis_K3	$K_3(\Delta u_L, r)$	(Xu 2022h)	(37)	16,28
20_Pairwise_velocity_generalized_kurtosis_K4	$K_4(\Delta u_L, r)$	(Xu 2022h)	(37)	15,27
21_Pairwise_velocity_generalized_kurtosis_K5	$K_5(\Delta u_L, r)$	(Xu 2022h)	(37)	16
22_Pairwise_velocity_generalized_kurtosis_K6	$K_6(\Delta u_L, r)$	(Xu 2022h)	(37)	15,27
23_Pairwise_velocity_generalized_kurtosis_K7	$K_7(\Delta u_L, r)$	(Xu 2022h)	(37)	
24_Pairwise_velocity_generalized_kurtosis_K8	$K_8(\Delta u_L, r)$	(Xu 2022h)	(37)	15,27
25_Particle_logdensity_correlation_for_yita	$<\eta\eta'>$	(Xu 2022h)	(2)	
26_Particle_density_delta_on_scale_r	$<\delta>$	(Xu 2022f)	(110)	13
27_Particle_logdensity_yita_on_scale_r	$<\eta>$	(Xu 2022f)		
28_Particle_pairs_at_z=0_r=0.1Mpc_h_u_and_r	**u** and **u'**	(Xu 2022h)		25
29_Particle_pairs_z=0_r=1.3Mpc_h_u_and_r	**u** and **u'**	(Xu 2022h)		26
30_Particle_potential_correlation_phi	$<\phi\phi'>$	(Xu 2022e)	(128)	
31_Particle_potential_phi_on_scale_r	$<\phi>$	(Xu 2022e)		
32_Transverse_velocity_correlation_rho_T	$\rho_T(r,z)$	(Xu 2022e)	(20)	16
33_Velocity_correlation_function_L20	$L_{(2,0)}=L_2$	(Xu 2022e)	(17)	2,3,4,7
34_Velocity_correlation_function_L30	$L_{(3,0)}=L_3$	(Xu 2022f)	(6)(46)	2,3
35_Velocity_correlation_function_L32	$L_{(3,2)}=R_{31}$	(Xu 2022f)	(8)(46)	2,3,8,12
36_Velocity_correlation_function_L40	$L_{(4,0)}$	(Xu 2022f)	(46)	2,4
37_Velocity_correlation_function_L42	$L_{(4,2)}$	(Xu 2022f)	(46)	2,4
38_Velocity_correlation_function_L50	$L_{(5,0)}$	(Xu 2022f)	(46)	2
39_Velocity_correlation_function_L52	$L_{(5,2)}$	(Xu 2022f)	(46)	2
40_Velocity_correlation_function_L54	$L_{(5,4)}$	(Xu 2022f)	(46)	2,5,10,12
41_Velocity_correlation_function_L60	$L_{(6,0)}$	(Xu 2022f)	(46)	2
42_Velocity_correlation_function_L62	$L_{(6,2)}$	(Xu 2022f)	(46)	2
43_Velocity_correlation_function_L64	$L_{(6,4)}$	(Xu 2022f)	(46)	2
44_Velocity_correlation_function_R21	$R_{(2,1)}=R_2$	(Xu 2022e)	(16)	2,3,5,8
45_Velocity_correlation_function_R31	$R_{(3,1)}=R_3$	(Xu 2022f)	(7)(45)	2,3
46_Velocity_correlation_function_R41	$R_{(4,1)}$	(Xu 2022f)	(45)	2,4
47_Velocity_correlation_function_R43	$R_{(4,3)}$	(Xu 2022f)	(45)	2,4,11,12
48_Velocity_correlation_function_R51	$R_{(5,1)}$	(Xu 2022f)	(45)	2
49_Velocity_correlation_function_R53	$R_{(5,3)}$	(Xu 2022f)	(45)	2
50_Velocity_correlation_function_R61	$R_{(6,1)}$	(Xu 2022f)	(45)	2
51_Velocity_correlation_function_R63	$R_{(6,3)}$	(Xu 2022f)	(45)	2
52_Velocity_correlation_function_R65	$R_{(6,5)}$	(Xu 2022f)	(45)	2,11
53_Velocity_correlation_function_T20	$T_{(2,0)}=T_2$	(Xu 2022e)	(18)	2,3,5,6
54_Velocity_correlation_function_T30	$T_{(3,0)}$	(Xu 2022f)	(47)	3
55_Velocity_correlation_function_T40	$T_{(4,0)}$	(Xu 2022f)	(47)	4
56_Velocity_correlation_function_T42	$T_{(4,2)}$	(Xu 2022f)	(47)	4
57_Velocity_dispersion_function_Sigma2_u	$\sigma_u^2(r,z)$	(Xu 2022e)	(27)	9
58_Velocity_moment_function_sum_uL_uLs_2	$<\Sigma u_L^2>$	(Xu 2022h)	(38)	19,20
59_Velocity_moment_function_sum_uL_uLs_4	$<\Sigma u_L^4>$	(Xu 2022h)	(38)	15
60_Velocity_moment_function_sum_uL_uLs_6	$<\Sigma u_L^6>$	(Xu 2022h)	(38)	15
61_Velocity_moment_function_sum_uL_uLs_8	$<\Sigma u_L^8>$	(Xu 2022h)	(38)	15
62_Velocity_moment_function_uL2	$<u_L^2>$	(Xu 2022h)		19,20
63_Velocity_moment_function_uL3	$<u_L^3>$	(Xu 2022h)		
64_Velocity_moment_function_uL4	$<u_L^4>$	(Xu 2022h)		15
65_Velocity_moment_function_uL5	$<u_L^5>$	(Xu 2022h)		
66_Velocity_moment_function_uL6	$<u_L^6>$	(Xu 2022h)		15
67_Velocity_moment_function_uL7	$<u_L^7>$	(Xu 2022h)		
68_Velocity_moment_function_uL8	$<u_L^8>$	(Xu 2022h)		15
69_Velocity_moment_function_uT2	$<u_T^2>$	(Xu 2022h)		20
70_Velocity_structure_function_S1LP	S_1^{lp}	(Xu 2022h)	(39)	18
71_Velocity_structure_function_S2i	S_2^i	(Xu 2022e)	(67)	14
72_Velocity_structure_function_S2L	S_2^l	(Xu 2022e)	(55)	24
73_Velocity_structure_function_S2LP	S_2^{lp}	(Xu 2022h)	(39)	21,22,23
74_Velocity_structure_function_S2x	S_2^x	(Xu 2022e)	(72)	12
75_Velocity_structure_function_S3LP	S_3^{lp}	(Xu 2022h)	(39)	23
76_Velocity_structure_function_S4LP	S_4^{lp}	(Xu 2022h)	(39)	23
77_Velocity_structure_function_S5LP	S_5^{lp}	(Xu 2022h)	(39)	23
78_Velocity_structure_function_S6LP	S_6^{lp}	(Xu 2022h)	(39)	23
79_Velocity_structure_function_S7LP	S_7^{lp}	(Xu 2022h)	(39)	23
80_Velocity_structure_function_S8LP	S_8^{lp}	(Xu 2022h)	(39)	23
81_Velocity_structure_function_S9LP	S_9^{lp}	(Xu 2022h)	(39)	23

p	$q=0$	$q=1$	$q=2$	$q=3$	$q=4$	$q=5$
1	$L_{(1,0)} = \langle u'_L \rangle$					
2	$L_{(2,0)} = \langle u_L u'_L \rangle$	$R_{(2,1)} = \langle \mathbf{u} \cdot \mathbf{u}' \rangle$				
3	$L_{(3,0)} = \langle u_L^2 u'_L \rangle$	$R_{(3,1)} = \langle u_L \mathbf{u} \cdot \mathbf{u}' \rangle$	$L_{(3,2)} = \langle u^2 u'_L \rangle$			
4	$L_{(4,0)} = \langle u_L^3 u'_L \rangle$	$R_{(4,1)} = \langle u_L^2 \mathbf{u} \cdot \mathbf{u}' \rangle$	$L_{(4,2)} = \langle u^2 u_L u'_L \rangle$	$R_{(4,3)} = \langle u^2 \mathbf{u} \cdot \mathbf{u}' \rangle$		
5	$L_{(5,0)} = \langle u_L^4 u'_L \rangle$	$R_{(5,1)} = \langle u_L^3 \mathbf{u} \cdot \mathbf{u}' \rangle$	$L_{(5,2)} = \langle u^2 u_L^2 u'_L \rangle$	$R_{(5,3)} = \langle u^2 u_L \mathbf{u} \cdot \mathbf{u}' \rangle$	$L_{(5,4)} = \langle u^4 u'_L \rangle$	
6	$L_{(6,0)} = \langle u_L^5 u'_L \rangle$	$R_{(6,1)} = \langle u_L^4 \mathbf{u} \cdot \mathbf{u}' \rangle$	$L_{(6,2)} = \langle u^2 u_L^3 u'_L \rangle$	$R_{(6,3)} = \langle u^2 u_L^2 \mathbf{u} \cdot \mathbf{u}' \rangle$	$L_{(6,4)} = \langle u^4 u_L u'_L \rangle$	$R_{(6,5)} = \langle u^4 \mathbf{u} \cdot \mathbf{u}' \rangle$

Figure 2. Two-point velocity correlation functions of different order (p,q). Kinematic relations are developed between correlation functions of same order p. Dynamic relations can be developed between correlation functions of different order p (Xu 2022f)